# Improved Reverse Bias Stability in p-i-n Perovskite Solar Cells with Optimized Hole Transport Materials and Less Reactive Electrodes

*Fangyuan Jiang,[1] Yangwei Shi,[1,2] Tanka R. Rana,[3] Daniel Morales,[4] Isaac Gould,[4] Declan P. McCarthy,[5] Joel A. Smith,[6] M. Greyson Christoforo,[6] Muammer Y. Yaman,[1] Faiz Mandani,[7] Tanguy Terlier,[8] Hannah Contreras,[1] Stephen Barlow,[5] Aditya D. Mohite,[9] Henry J. Snaith,[6] Seth R. Marder,[4,5,10] J. Devin MacKenzie,[3,11] Michael D. McGehee,[4,5,10] David S. Ginger[1]**

[1] Department of Chemistry, University of Washington, Seattle, WA 98195, USA

[2] Molecular Engineering & Sciences Institute, University of Washington, Seattle, WA 98195, USA

[3] Department of Materials Science and Engineering, University of Washington, Seattle, WA 98195, USA

[4] Materials Science and Engineering Program, University of Colorado Boulder, Boulder, CO 80309, USA

[5] Renewable and Sustainable Energy Institute, University of Colorado Boulder, Boulder, CO 80303, USA

[6] Department of Physics, University of Oxford, Parks Road, Oxford OX1 3PU, UK

[7] Department of Chemical and Biomolecular Engineering, Rice University, Houston, TX 77005, USA

[8] SIMS Laboratory, Shared Equipment Authority, Rice University, Houston, TX 77005, USA

[9] Department of Materials Science and NanoEngineering, Rice University, Houston, TX 77005, USA

[10] Department of Chemical and Biological Engineering and Department of Chemistry, University of Colorado Boulder, Boulder, CO 80303, USA

[11] Department of Mechanical Engineering, University of Washington, Seattle, WA 98195, USA

***** Corresponding author email: dginger@uw.edu

## Abstract

As perovskite photovoltaics stride towards commercialization, reverse bias degradation in shaded cells that must current match illuminated cells is considered a serious challenge. Previous research has emphasized the role of iodide and silver oxidation, and the role of hole tunneling from the electron transport layer into the perovskite to enable the flow of current under reverse bias in causing degradation. Here we show that device architecture engineering has a significant impact on the reverse bias behavior of perovskite solar cells. By implementing both a ~35-nm-thick conjugated polymer hole transport layer, and a more electrochemically stable back electrode, we demonstrate average breakdown voltages exceeding -15 V, comparable to those of silicon cells. Our strategy for increasing the breakdown voltage reduces the number of bypass diodes needed to protect a solar module that is partially shaded, which has been proven to be an effective strategy for silicon solar panels.


## ToC graphic

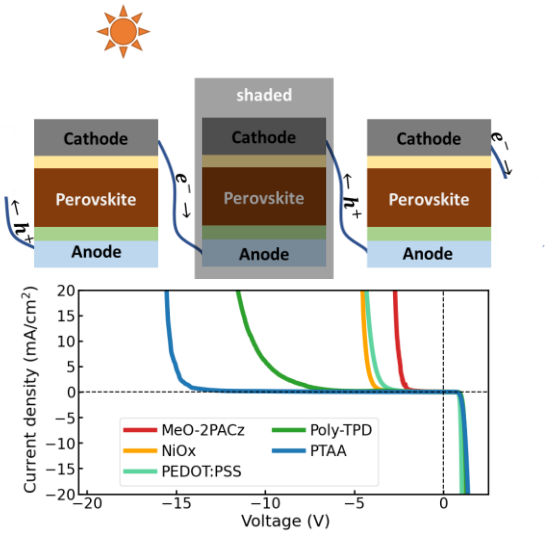

## Main

Metal halide perovskite solar cells, with certified power conversion efficiencies (PCE) exceeding 26% (single junction) and 33% (perovskite-silicon tandem),[1] have emerged as competitive single-junction rivals to, and ideal tandem partners with the monocrystalline silicon solar cells that have dominated the photovoltaic (PV) market for decades. Early on, most efforts were directed at making perovskite cells more efficient.[2–11] Recently, as the efficiency of perovskite PV made using low-energy and low-capital-cost processes has begun to match and even exceed that of silicon PV, more efforts have been directed at issues of stability, with solar cells maintaining > 90% initial PCE after a few thousands of hours' aging at different ISOS (the International Summit on Organic Photovoltaic Stability) conditions,[12–14] and with various consortia emerging to develop testing protocol and recommendations for halide perovskite PV modules.[15]

Recently, a number of reports have highlighted reverse bias stability as a critical issue facing perovskite PV, perhaps even the most demanding durability issue for fielded solar modules.[16–28] Reverse bias instability occurs when the low-output solar cells (e.g., due to partial shading) in serially connected modules are forced to match the current output of other high-output solar cells. The resulting voltage and current flow can accelerate device degradation via many mechanisms, from undesired electrochemical reactions to local heating. The resulting device failures are a major concern even for well-established silicon PV technologies. So far, relatively few reports have studied the reverse bias stability of perovskite solar cells. From a device engineering perspective, there are two main strategies for improving the reverse bias stability: one is to fabricate solar cells that do not degrade when passing high reverse *current* ($J_{mpp}$, the current density at the maximum power point). While proposed in literature,[20] this approach is not used in any commercial technologies, and has not yet seen widespread success in halide perovskites.[18] A second, more common approach, is to stabilize solar cells at high reverse *bias*, typically via improving the breakdown voltages ($V_{rb}$s), so as to minimize the use of bypass diodes needed to protect a solar panel.[29] This approach, widely seen in commercial silicon PV,[30,31] is discussed and studied more often for perovskite PV at present.[16,17,21] However, the $V_{rb}$s in the perovskite solar cell studies typically range from -0.5 V to -3 V,[19–28,32–35] which lag significantly behind typical silicon PV $V_{rb}$ value of -13 V.[21,36] Some recent studies have reported device architecture engineering, via building perovskite-silicon tandems[21,27] or employing a mesoscopic solar cell structure with carbon electrode[22], as potential approaches to circumvent the reverse bias challenge of perovskite PV. Nevertheless, there is a need for new pathways to increase $V_{rb}$ and stabilize the perovskite solar cell itself at higher reverse bias in order to reduce the number of bypass diodes and thus make both single-junction and tandem cells much more cost-effective.[16,21]

There are multiple ways in which different types of p-i-n structured perovskite solar cells degrade under reverse bias. An incomplete understanding of these mechanisms and the factors that promote them is a major challenge towards addressing the reverse bias instability issue in perovskite solar cells. In some

cells the current increases very abruptly at a voltage as low as -0.2 V and thermal imaging reveals localized hot spots. We will show in a separate study that dielectric breakdown in defective regions of the cells can explain these observations. Nevertheless, in terms of *early-stage* device performance loss, the predominant models garnering attention in the field today suggest that under reverse bias, halide ions accumulated at the perovskite/electron-transport layer (ETL) interfaces result in sharp enough band bending to allow holes to tunnel from the ETL into the perovskite.[20,35] Several reports propose that under these conditions iodide is oxidized,[23,35,37] which could increase the mobility of iodine species and enhance the escape of these species from the perovskite layer.[35] However, in the presence of Ag electrode, injected holes will oxidize Ag rather than iodide, given the reactive nature of Ag.[37] These models indeed explain many features observed to date, including the presence of Ag in the perovskite layer following reverse bias,[27,37] and the improvement in reverse bias stability when tailoring the interface between the perovskite and the ETL.[23] While those experiments are consistent with the model, perovskite solar cells still suffer serious reverse bias degradation, with obvious device performance loss even after stressing the cells at -1 V for 10 min,[23] and with $V_{rb}$ being far below that of silicon PV.[21,36] Meanwhile, in contrast to the focus on oxidation events, there has been far less discussion on the nature of the reduction events that must occur somewhere else in the cell to prevent oxidation events from building up net charge in the device under reverse bias.

Here, we systematically investigate the reverse bias behavior of typical p-i-n structured perovskite solar cells. Our results show that using thicker conjugated polymer films as the hole-transport layer (HTL) can lead to dramatic increases in $V_{rb}$s. Even with electrochemically reactive Ag electrodes, using a thick polymer PTAA HTL can improve the $V_{rb}$ to -8 V, as compared to -1 V for phosphonic-acid-modified ITO interfaces that are in wide use today. Furthermore, replacing Ag with more electrochemically stable Au, we demonstrate record $V_{rb}$ exceeding -15 V for perovskite solar cells, which is comparable to that for silicon solar cells and is much better than that for other PV technologies.[17,36] As a result, our optimized perovskite solar cells demonstrate recoverable performance after stressing at -7 V for 9 hours both in the dark and under partial illumination. Based on these experimental observations, we revisit previous proposals of reverse bias-driven degradation mechanisms,[19,20,23,35,37] and propose that planarization of the ITO electrode to prevent perovskite from touching ITO, blocking of electron injection, and use of electrochemically stable electrodes need to be considered as important parts of the complete picture of reverse bias-driven device degradation behavior.

## Reverse bias behavior in typical p-i-n perovskite solar cell

We start this reverse bias stability study with an archetypal p-i-n structured perovskite solar cell **(Fig. 1a)**. We use a mixed-cation, triple-halide perovskite composition with the formula of $Cs_{0.22}FA_{0.78}Pb(I_{0.85}Br_{0.15})_3$ with 3 mol % of $MAPbCl_3$ additive, where FA refers to formamidinium and MA refers to methylammonium. This perovskite composition has a relatively wide bandgap of ~1.67 eV suitable for perovskite-silicon tandems.[38–46] We choose a [2-(3,6-dimethoxy-9*H*-carbazol-9-yl)ethyl]phosphonic acid (MeO-2PACz) self-assembling monolayer (SAM) as the reference hole transporting interface modifier and archetypal $C_{60}$ as the ETL because they are commonly used and provide good device performance in previous reports.[41,47–49] We also employ Ag as a representative widely-used back electrode. In the reverse-bias regime, we ground the Ag electrode, and apply a negative bias to the indium tin oxide (ITO) electrode. In this case, electrons will be injected from the cathodic ITO electrode and holes from the anodic Ag electrode.

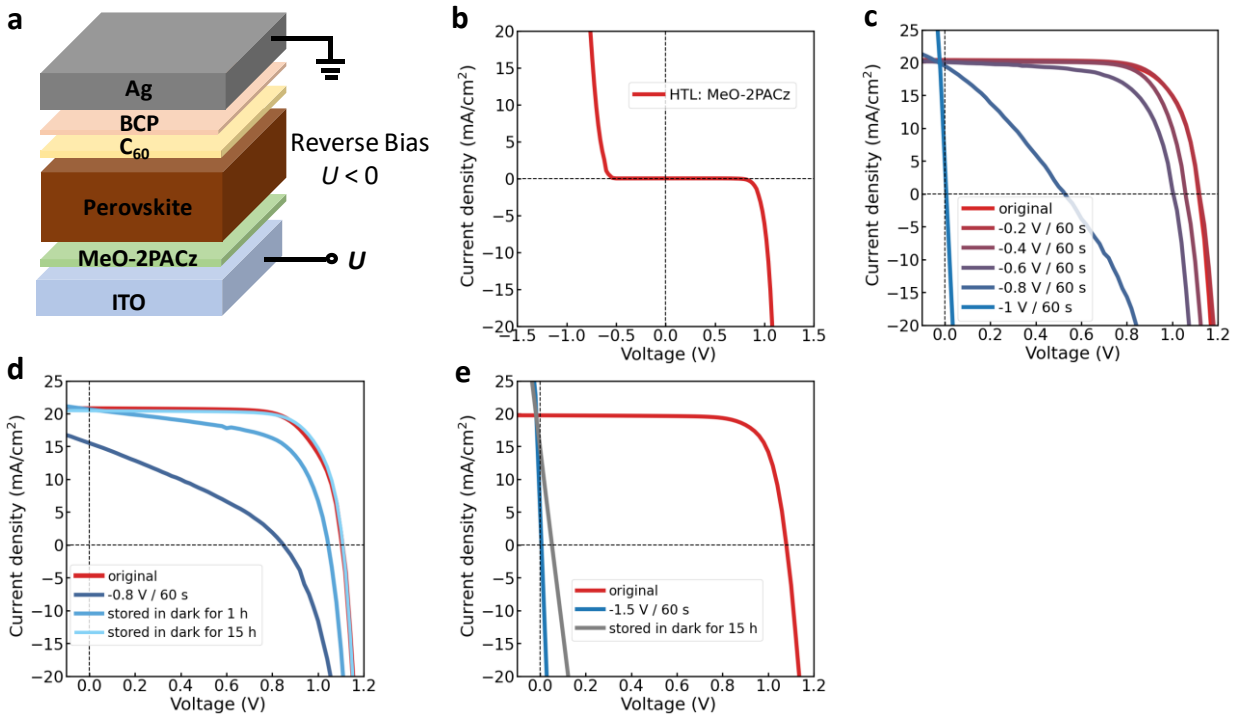


**Fig. 1 | Reverse bias stability study in an archetypal p-i-n structured perovskite solar cell. a**, Schematic diagram of the as-fabricated perovskite solar cell. **b**, Representative dark *J-V* curves of the as-fabricated perovskite solar cell. **c**, *J-V* curves (reverse scans) of the perovskite solar cell after holding at the stated reverse bias (gradually increased) for 60 s. **d**, *J-V* curves (reverse scans) showing that after biasing at -0.8 V for 60 s, device performance can be restored after overnight (~15 h) dark storage. **e**, *J-V* curves (reverse scans) showing that device performance cannot be recovered after biasing at -1.5 V for 60 s. During the reverse bias stressing test, a current compliance of $J_{mpp}$ (~ 19 mA/cm$^2$) was set to limit the maximum current flowing through the cell.

**Supplementary Figs. 2b** and **3** show the current density – voltage (*J-V*) scans and device performance statistics of the as-fabricated solar cells under forward and reverse scans. The best power conversion efficiencies (PCE) are over 18% for both reverse and forward scans, consistent with expectations for this device stack.[50] We then investigate the reverse-bias behavior of these solar cells by measuring their dark *J-V* curves **(Fig. 1b** and **Supplementary Figs. 4b** and **9)**, and identify the breakdown voltage $V_{rb}$s, defined as the onset voltage where the reverse current starts to increase dramatically **(Supplementary Fig. 4)**, to be around -0.7 V.

To monitor the reverse bias induced degradation, we adopt a stress test where we progressively increased the reverse bias in increments of -0.2 V. We note that, throughout the manuscript, we always refer to an increase in reverse bias as the increase in its absolute value (more negative), with low reverse bias meaning that the absolute value is low. After each step, we measure *J-V* curves under simulated 1-sun illumination to monitor the device performance changes (**Fig. 1c**, reverse scans). As the reverse bias increases, the solar cell degrades more until it undergoes complete performance loss after being stressed at ~ -1 V. Consistent with previous studies,[19] we find that, with a limited short-time stressing, the solar cell performance loss undergoes two stages: if the reverse bias is low with low current (< ~1 mA/cm$^2$) passing, the solar cell can recover its performance after the removal of the bias **(Fig. 1d)**. On the contrary, if the reverse bias is high with obvious current (> ~1 mA/cm$^2$) flowing, the solar cell will lose performance irreversibly and/or become shunted **(Fig. 1e)**.

Previous reports have identified the electrochemical oxidation of the Ag electrode,[19,27,37] and the interaction between iodide and injected holes,[23,37] as major contributors to device degradation under reverse bias. Bertoluzzi *et al*. conducted drift-diffusion simulations to show that holes tunnel into the perovskite and subsequently react with iodide, due to sharp band bending near the perovskite/ETL contact.[35,51] These factors all point to the key role of the interfaces at the perovskite/ETL/metal electrode side. In particular, Ni *et al.* reported that the introduction of a hole-blocking layer between the perovskite and $C_{60}$ suppresses the interaction between iodide interstitials and injected holes, improving reverse bias stability.[23] Therefore, we first focused our attempts on optimizing the interface between perovskite and $C_{60}$. Among various strategies, we attempted passivating the perovskite surface with (3-aminopropyl)trimethoxysilane (APTMS) which has been proven to reduce surface recombination velocities at both neat perovskite[52] and perovskite/fullerene interfaces[49], as well as suppress bias-induced or light-induced shifts in the surface potential.[53,54] All these observations suggest that APTMS can reduce halide vacancies and vacancy-mediated halide transport at the surface, which should, in theory, suppress the ionic conductivity of the perovskite, and therefore the ability of hole tunneling, and halide ions to diffuse and react at the interface of $C_{60}$ and Ag.[35] In addition, we attempted inserting an additional non-fullerene ETL to possibly block the ion diffusion into $C_{60}$ or increase the physical barrier for hole injection, as well as slow down possible

reactions of the halide with the fullerene.[55,56] **Supplementary Fig. 5** compares the typical *J-V* curves and reverse bias behaviors of reference and APTMS-passivated solar cells. While APTMS surface treatment indeed improves the $V_{OC}$,[49,52] we did not observe any device stability improvement under reverse bias. Similarly, **Supplementary Fig. 6** shows that the additional ETL, a naphthalene diimide derived polymer named NDI-1,[57] also has no beneficial impact on the reverse bias behavior. These experimental observations led us to consider that there might be other degradation pathways which are more preferential/important than those induced by non-ideal perovskite/$C_{60}$ interface, and there should be other pathways to improve $V_{rb}$.

## Polymer HTLs dramatically improve $V_{rb}$s

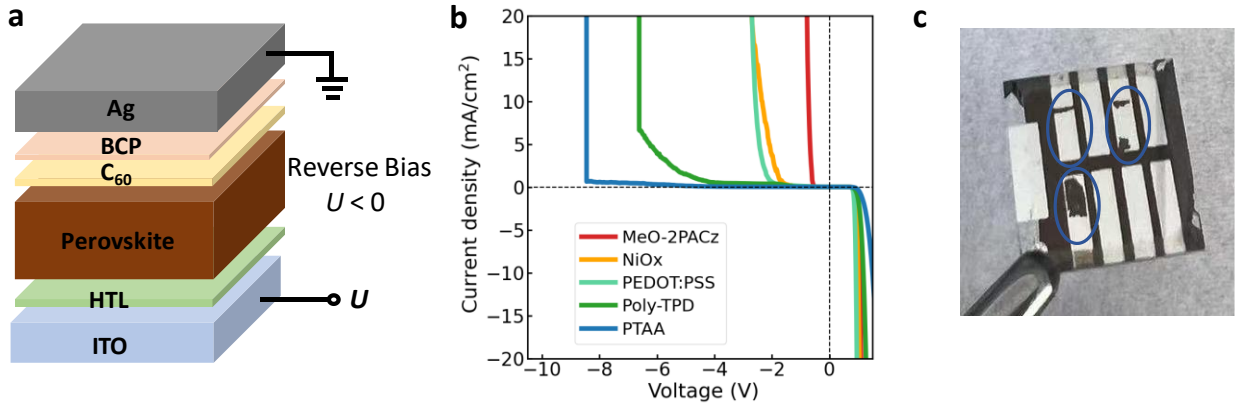


**Fig. 2 | The effect of different HTLs on $V_{rb}$s. a**, Schematic diagram of a typical p-i-n structured perovskite solar cell under reverse bias. **b**, Dark *J-V* curves showing that different HTLs lead to different reverse bias behavior. **c**, Image of PTAA-based perovskite solar cells (marked regions) after dark *J-V* sweeping to exceed $V_{rb}$.

We next explore whether replacing the commonly used phosphonic acid HTL could improve solar cell stability under higher reverse bias. This choice may seem surprising since, according to the mainstream models for explaining reverse bias degradation (Ag oxidation by injected holes[19,27,37] or iodide oxidation via hole tunneling from ETL to perovskite[20,23,35,37]), changing the HTL is not expected to have a significant effect on $V_{rb}$. However, if the ITO touches perovskite in regions where the thin phosphonic acid HTLs are defective or that they simply cannot block electrons, then injected electrons from ITO may induce reduction events (for instance, from $Pb^{2+}$ to $Pb^0$ [58]) to cause the above-mentioned device degradation behavior. To see if we could prevent such a process, we compared five different HTLs (molecular structures shown in **Supplementary Fig. 1**), including the reference phosphonic acid MeO-2PACz, $NiO_X$, poly(3,4-ethylenedioxythiophene) polystyrene sulfonate (PEDOT:PSS), poly(4-butyl-triphenylamine-4',4"-diyl) (Poly-TPD), and poly(2,4,6-trimethyltriphenylamine-4',4"-diyl) (PTAA). We optimized the processing of

perovskite films on top of these HTLs to ensure good crystallinity and morphology **(Supplementary Figs. 7** and **8)**, as well as the processing condition of these HTLs to ensure good device performance **(Supplementary Figs. 2, 3** and **Table 1)**. We measured thicknesses of MeO-2PACz, $NiO_X$, PEDOT:PSS, Poly-TPD, PTAA as <5 nm (presumably monolayer[59,60]), 40 nm, 29 nm, 16 nm, and 35 nm respectively. We also introduced an additional PFN-Br layer (< 5 nm) on the top surface of PTAA and Poly-TPD to increase the wettability of the perovskite solution (see **Supplementary information** for experimental details and control experiments).

**Figure 2b** shows that these HTLs do lead to significantly different solar cell reverse bias behaviors. We chose the dark *J-V* curves displayed in this study to be representative: we found that the majority of the cells, before reaching $V_{rb}$s, experience gradual increase in current, while a smaller portion of the cells show an abrupt increase in current. The different shapes of these dark *J-V* curves might indicate different device breakdown pathways as we discuss in **Supplementary Information**. Considering this, to facilitate practical analysis and remove selection bias, we used a computer code to extract the $V_{rb}$s from over 360 *J-V* curves automatically for this study (**Supplementary Table 2**). We show resulting $V_{rb}$ statistics of cells with different HTLs in **Supplementary Fig. 9** and **Table 2,** where $V_{rb}$ values are **-1.03 ± 0.51** V for MeO-2PACz, **-1.82 ± 0.40** V for $NiO_X$, **-2.93 ± 0.46** V for PEDOT:PSS, **-5.30 ± 1.87** for Poly-TPD, and **-7.60 ± 0.94** V for PTAA-based perovskite solar cells. We see that the MeO-2PACz exhibits a much smaller $V_{rb}$s than other counterparts, especially polymers (PEDOT:PSS, PTAA, Poly-TPD). We note that PEDOT:PSS, being a mixed ionic-electronic conductor with electrochemical reactivity,[61] possibly contains other ion components that are susceptible to react with perovskite, which is consistent with the much lower $V_{rb}$s of PEDOT:PSS compared to other polymer HTLs PTAA and Poly-TPD. We also note our results are consistent with previous perovskite photodetector work by Li[62] and Tsai[63], as well as a recent perovskite solar cell study by Henzel[64], where improved $V_{rb}$s were achieved in devices that all coincidentally used PTAA HTL. Even though our results differ from these studies in terms of materials and strategies, having a robust PTAA interlayer seems to be a common characteristic to achieve larger $V_{rb}$s.

For PTAA-based solar cells, as we further increase the bias to exceed the $V_{rb}$ during the *J-V* sweeping (**Supplementary Fig. 11)**, we observe catastrophic failure of the cells that is sufficiently severe to be visible by the naked eye **(Fig. 2c)**. Scanning electron microscopy **(Supplementary Fig. 12)** confirms that the cells were severely damaged following reverse bias stressing, especially at the Ag electrode.

## Electrochemically stable electrode yields even greater $V_{rb}$s

Ag is relatively easy to oxidize, especially in the presence of halide species,[65] and is a fairly soft metal with relatively mobile cations. Therefore, to test whether the electrochemistry of Ag aggravates the reverse bias-induced solar cell degradation,[37] we fabricated solar cells using more electrochemically stable Au as the back metal **(Fig. 3a)**. **Supplementary Fig. 13 and Table 1** first show that all these solar cells display good device performance. **Figure 3b** clearly demonstrates that replacing Ag with Au in the back electrode yields even greater improvements in $V_{rb}$s. We measured the dark *J-V* curves and identified the $V_{rb}$s to be -2.28 ± 0.76 V for MeO-2PACz, -3.74 ± 0.49 V for $NiO_X$, -3.69 ± 0.39 V for PEDOT:PSS, -9.42 ± 1.61 V for Poly-TPD, and -15.36 ± 1.52 V for PTAA-based perovskite solar cells (**Supplementary Fig. 14** and **Table 2**). The average $V_{rb}$ increase from -2.28 V (MeO-2PACz) to -15.36 V (PTAA) again verifies that the choice of HTL can significantly improve the cell robustness to device degradation at high reverse bias. Notably, the average $V_{rb}$ exceeding -15 V achieved in PTAA-based perovskite solar cell is comparable to, or even better than values reported for commercial PV technologies, such as silicon, CIGS, and CdTe.[17,21,36] **Figure 3c** compares the reverse current on a log scale for different perovskite solar cells. The PTAA-based devices show much lower (~ a few orders of magnitude) reverse-bias dark current than that of other non-PTAA based solar cells. Importantly, we note that the $V_{rb}$s for all the Au-based perovskite solar cells are better than that of the Ag-based cells made with the same HTLs, suggesting that the $V_{rb}$ *may depend on interactions spanning both interfaces*. We explore this observation further below.

We also investigate the reverse bias behaviors of perovskite solar cells when illuminated with dim light (< 0.1 Sun), as shown in **Supplementary Figs. 18** and **19**. Such illumination serves to simulate the real outdoor environment for solar modules when the low power-output cells are not shaded under complete darkness. We find that, in the presence of < 0.1 Sun illumination, the $V_{rb}$s, are -2.4 V with MeO-2PACz **(Supplementary Fig. 18c)** and ~ -14 V with PTAA **(Supplementary Fig. 19c – d** and **Table 2)**, remaining similar with that in complete darkness. We also tested the $V_{rb}$s of the PTAA based solar cells at 45 °C, and obtained an average $V_{rb}$ value still exceeding -15 V (**Supplementary Fig. 22** and **Table 2**).

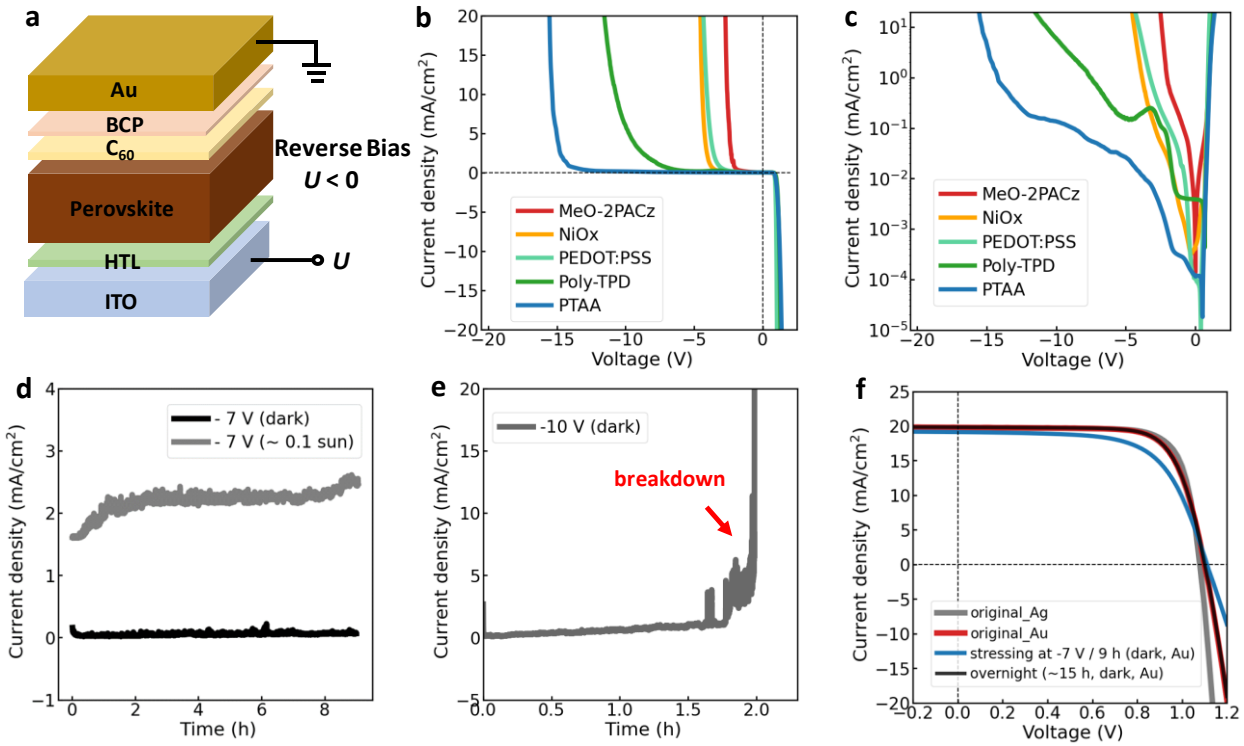


**Fig. 3 | The effect of electrochemically stable Au electrode on $V_{rb}$s. a**, Schematic diagram of the p-i-n structured perovskite solar cell employing Au as the top electrode, under reverse bias. **b,** Linear and **c**, log scale dark *J-V* curves of perovskite solar cells with different HTLs. **d,** Current density tracking of PTAA-based perovskite solar cells stressed at -7 V for 9 h in the dark or under ~0.1 Sun dim light illumination. **e**, Current density tracking of PTAA-based perovskite solar cells stressed at -10 V for 9 h in the dark where solar cell breakdown takes place at around ~2 h. **f**, *J-V* curves (reverse scans) showing that device performance can be restored after aging at -7 V for 9 h.

We note that reverse bias induced device degradation is not only related to the *magnitude*, but also the *duration* of the applied bias, as there is an obvious dependence of the device degradation rate and reverse bias current.[64] Thus, to show that the improved stability with PTAA HTL is not an artifact of scan rates, we study the reverse bias behavior of PTAA-based perovskite solar cells over an extended duration. **Figure 3d** tracks the reverse current densities of perovskite solar cells aged at -7 V for 9 h in the dark (< ~0.1 mA/cm$^2$) and under dim light (~ 0.1 Sun illumination, < ~2.5 mA/cm$^2$). We can see that the current densities remain low across the whole stressing window. In contrast, as we increase the bias to -10 V **(Fig. 3e)**, the reverse current density initially remains low/stable (< ~0.2 mA/cm$^2$), but dramatically increases after around 2 h. Such a *sudden* reverse current increase is very likely a result of device shunting, which we hypothesize could be related to metallic Pb formation and could be a target for future characterization.

We also conduct *J-V* measurements to monitor the performance changes of PTAA-based solar cells after stressing at high bias for different durations. While negligible device degradation occurs when solar

cells are stressed at -7 V for a relatively short duration of 1800 s (30 min) **(Supplementary Fig. 23b)**, extending the duration to 9 h leads to slight device performance loss (**Fig. 3f** and **Supplementary Fig. 23c)**. Notably the device performance is recoverable even under such lengthy exposure at high reverse bias. As we increase the bias to -10 V, the perovskite solar cell starts to show obvious degradation after aging for 10 min (reverse current density < ~0.2 mA/cm$^2$), which, fortunately, is mostly recoverable after only 10 min under illumination and *entirely recoverable* after dark storage, as shown in **Supplementary Fig. 23d**. We also discuss the resilience of the PTAA-based cells against multiple cycles of reverse bias stressing in **Supplementary Fig. 24**, and the device performance loss under high reverse bias and recovery mechanism in **Supplementary Information.**

## Reverse bias degradation mechanism

From the above observations, we conclude that *the choice of HTLs and metal electrode has a large impact on the reverse bias current-voltage curve and the consequently the amount of degradation that takes place at certain voltages.* Given the previous emphasis on the perovskite/ETL interface[23,35,37] and the strong experimental evidence that oxidation reactions are occurring under reverse bias (i.e., considerably enhanced Ag signals in the perovskite layer based on Time-of-Flight Secondary Ion Mass Spectrometry (ToF-SIMS) depth profile[37] and cross-sectional scanning transmission electron microscopy-energy dispersive X-ray spectroscopy[27], observation of halide segregation using photoluminescence (PL) spectroscopy,[19,37] as well as identification of chemical nature changes of mobile defects based on drive-level capacitance profiling technique[23]), the dramatic influence of the HTLs on reverse bias stability is very surprising. Thus, we consider why the choice of polymer HTLs could make such a huge difference by examining four main hypotheses: (1) the polymer HTLs could somehow store reactive halogen species,[66] therefore delaying the onset of permanent performance loss; (2) the polymer HTLs could somehow drop a substantial fraction of the reverse voltage, reducing the field experienced by the perovskite and thus indirectly suppressing hole injection at the anodically-biased ETL interface; (3) the role of electron injection under reverse bias has been overlooked, and these HTLs' ability in blocking electron injection from ITO to perovskite under reverse bias are different, and/or (4) the possibility that the thick polymer HTLs provides a physical barrier to reduce shorting/shunting at imperfections in the device.

Ultimately, we dismiss the first two hypotheses in favor of the third and fourth (**Supplementary Figs. 26 - 30**, with detailed calculations and analyses). First, when considering the role of the polymer HTLs as a possible halide "sponge",[66] we note that even a "deep-HOMO" polymer like poly(*N*-vinylecarbazole) (PVK) still improves the $V_{rb}$s significantly **(Supplementary Fig. 26)**. This observation effectively rules out iodide/polymer HTL reactions as the source of improved reverse bias stability. Second, we examine the effects of the thicker HTLs on the electric field distribution in the device, using both back-of-the-envelope

calculation **(Supplementary Fig. 27)**, full drift-diffusion simulation **(Supplementary Fig. 28 – 29)**, as well as analyses of "PTAA de-doping" (**Supplementary Fig. 30)** and/or device *J-V* curves **(Supplementary Information)**. While there are a wide range of variables, such as that the electric field and the distance over which bands bend in the perovskite is dependent on the mobile ion species and densities,[35] we conclude that it is unlikely for the addition of even a "thick" polymer PTAA HTL to lead to the necessary changes in field profiles in the device – the PTAA HTL would need to drop >80% of the applied bias to cause the necessary $V_{rb}$s increase from -2.28 V (MeO-2PACz) to -15.36 V (PTAA) in this case. If the voltage drop across the HTL were that large, the devices would have a remarkably poor efficiency/performance.

We now discuss the possibility that the electron injection, which has been generally overlooked, is playing an essential role in controlling reverse bias-drive degradation of perovskite solar cells. Previous analytical results indicate that oxidation of the Ag electrode[27,37] and iodide species[23,35,37] have taken place. Nevertheless, *charge conservation requires that oxidation and reduction reactions occur in pairs*.[65] From a device physics perspective, oxidation without a corresponding reduction corresponds to injection of uncompensated positive space charges, which would lead to a large field that would oppose further hole injection. From an electrochemical perspective, these positive charges would correspond to an increase in the oxidation potential, slowing down further oxidation.

We estimated such an effect based on the Poisson equation (see **Supplementary information** for detailed calculations and analyses): an injected hole (oxidized species) density of ~1.4 x $10^{16}$ $cm^{-3}$, without corresponding electrons (reduction reaction), would be sufficient to completely counter an applied bias of 10 V across a 460-nm-thick perovskite film. Such a hole density corresponds to the oxidation of < 1% of a monolayer of Ag atoms at metal/ETL interface or the oxidation of ~0.00015% of the iodide in the perovskite. With these factors in mind, we propose a modification to the current picture of oxidation-driven degradation of p-i-n structured perovskite solar cell devices under reverse bias: we speculate that the metal electrode or iodide oxidation events do take place as previously reported,[19,23,35,37] *however, the progression of these oxidations must be paired with reduction events at the cathodically-biased HTL/perovskite interface*. Therefore, the ability of the HTLs to affect electron injection (reduction reactions) would have a direct impact on the oxidation reactions by preventing oxidation from progressing substantially when a paired reduction/electron injection event is missing.

We also consider that the role of PTAA in improving reverse bias stability may arise from its ability, given its polymeric nature and relatively thick thickness (~35 nm), to better homogenize/planarize the bottom transparent conductive oxide (TCO) contact. In the organic light-emitting diode (OLED) fields, it is well known that planarization of the TCO is essential for device stability and yield.[67–72] We believe that the thick PTAA HTLs are playing similar roles in perovskite PV, especially under reverse bias where the electric field and/or current would be concentrated on any imperfections, defects, pinholes, or dust particles

in the device and drive localized electrochemical breakdown. **Supplementary Fig. 31** shows that if we use rougher fluorine doped tin oxide (FTO) rather than ITO as the TCO, average $V_{rb}$ values drop to -1.09 V with PTAA HTL and Ag electrode (**Supplementary Table 2**). Similarly, if there are obvious defects, imperfections, pinholes and/or dust particles existing in the cells that lead to initial poor device performance (PCE < 10%), perovskite solar cells, with PTAA HTL and Au electrode, display an average $V_{rb}$ as low as -1.76 V (**Supplementary Fig. 32** and **Table 2**). We also analyzed the distribution of $V_{rb}$s and calculated the coefficient of variation of each HTL case (**Supplementary Fig. 33** and **Table 3**), and found that the coefficient of variation for the MeO-2PACz is the worst, and the coefficient of variation for PTAA-based devices is the best. These results highlight the importance of TCO planarization and refinement of device processing/fabrication to avoid pinholes/imperfect sites that serve as channels for device breakdown. We note that this mechanism, that thick PTAA HTL offers better TCO planarization, is not completely distinct from the role of thick polymer HTLs in physically blocking electron injection/tunneling and preventing electrochemical degradation pathways, and that thick polymer HTLs would synergistically provide both advantages.

We now discuss what the reduction reactions at the ITO/HTL/perovskite side could be. We speculate that the reduction of $Pb_i^{2+}$ (shadow defects) into $Pb_i^0$ (deep defects) by injected electrons is most likely. This is plausible as the reduction of $Pb^{2+}$ is electrochemically facile compared to halide oxidation or even reduction of silver halides salts.[65] This step is also consistent with the observation of PL quenching fronts propagating from the negatively-biased electrode in coinage-metal/perovskite junctions.[58] Such PL quenching has been proven to be reversible,[58] which is consistent with the observed recoverable device performance loss in our perovskite solar cells under low reverse bias regime with low current **(Fig. 1d)**. Furthermore, previous X-ray photoelectron spectroscopy measurements have confirmed that $Pb^0$ impurities usually exist in perovskite as a decomposition byproduct, and these $Pb^0$ impurities are generally associated with the degradation of solar cells.[73–75]

In **Fig. 4**, we propose a set of electrochemical reactions (oxidation – reduction pairs) that may occur under reverse bias in perovskite solar cells with Ag or Au electrodes. To better understand the degradation process, we present a more detailed schematic in **Supplementary Figs. 34 – 40** along with more analyses. We note that the perovskite degradation processes are very complex, thus we do not anticipate the electrochemical reactions proposed in this study to be the only/ultimate reactions, and we do not anticipate our model to be the only/ultimate mechanism. However, we put this framework forward as a self-consistent proposal that is supported by our experimental data here, as well as various analytical studies in the literatures.[19,23,35,37]

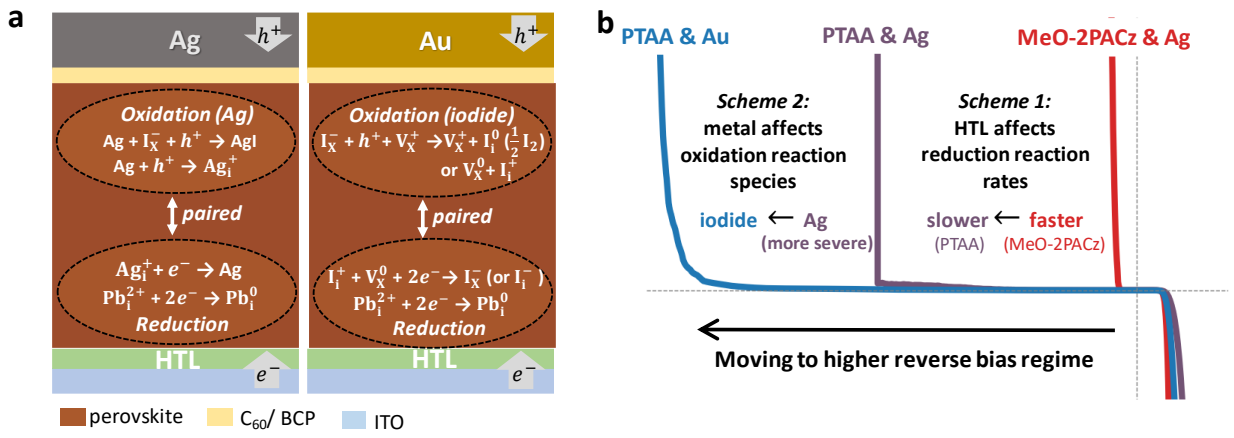


**Fig. 4 | Schematic of perovskite solar cell degradation mechanisms under reverse bias. a**, Proposed paired electrochemical reactions in perovskite solar cells with Ag or Au top electrode. **b**, Schematic suggesting that the role of PTAA HTLs is to slow down reduction reaction rate (thus the necessarily-paired oxidation reactions), while the role of Au electrode is to replace Ag oxidation with less severe/deadly iodide oxidation. Both strategies contributed to the record $V_{rb}$ in this study.

In a perovskite solar cell with a Ag electrode **(Fig. 4a, left)**, consistent with previous reports,[37] we believe that Ag oxidation will first take place at the Ag/BCP/$C_{60}$ interface to form AgI and $Ag_i^+$, given the relatively low oxidation potential of Ag in the presence of iodide,[65] and that iodide can diffuse into $C_{60}$ easily.[19,37] ToF-SIMS (**Supplementary Fig. 38**) and X-ray photoelectron spectroscopy (XPS, **Supplementary Fig. 40a**) confirm Ag oxidation (the formation of AgI, and the shift of the binding energies associated with Ag 3d, respectively) after reverse bias/current stressing (see detailed discussion in **Supplementary Information**). However, it is worth noting that significant Ag oxidation cannot proceed in the absence of necessarily paired reductions, according to our estimations based on Poisson equation as discussed above. In other words, *the electrochemical reactions, which are directly linked to solar cell degradation, rely on the reduction reaction (electron injection) rates at the HTL/perovskite interface*. Since different HTLs offer different levels of electron blocking, and since they also serve as different levels of physical barriers to reduce shorting/shunting at imperfections, a good HTL is therefore expected to slow down the reduction reaction rate and therefore slow down the necessarily paired oxidations at the anodically biased contact. Compared with MeO-2PACz (< 5 nm), through which electrons can transport/tunnel through easily, thick polymer PTAA layers (~35 nm) offer better electron blocking ability, therefore pushing the electrochemical degradation of perovskite solar cells to higher reverse bias regime, shown as ***Scheme 1*** in **Fig. 4b**. This is very plausible because PTAA-based solar cells demonstrate reverse currents that are a few orders lower than that of MeO-2PACz **(Supplementary Fig. 10a)**, consistent with the much slower electron injection in the case of PTAA HTL. ToF-SIMS results (**Supplementary Fig. 38**) confirm our hypothesis that improving a barrier at the HTL side, via use of thick PTAA layer, can slow down the

Ag oxidation rates on the opposite side: we see an obvious rise of the AgI signal at the Ag/BCP/$C_{60}$ interface after stressing the MeO-2PACz cell at -1 V for 2 hours, while we see negligible AgI signal change in PTAA based cell even if we stress the cell at -3 V for 2 hours. We note that the use of thicker polymer HTLs to stabilize the perovskite solar cells under higher reverse bias may sound surprising, it aligns with a recent analytical study by Bitton et al. where the authors also highlighted the choice of HTL layers in battling electrochemistry that induces degradation.[76] Our strategy of using thicker HTLs is also consistent with the study by Galatopoulos et al where the authors reported enhanced thermal stability in forward bias by lengthening the ETL.[77]

As the electron injection starts/increases at the ITO/HTL side, the progression of Ag oxidation becomes possible. In this case, more Ag will get oxidized to form AgI and/or $Ag_i^+$. Meanwhile, if the reverse bias increases with more injected carriers, $Ag_i^+$ ions could possibly drift along the electric field and get reduced to form metallic Ag, as claimed/characterized in previous literatures.[19,27,37] We note that, the presence of abundant Ag signals in perovskite cells (after reverse bias stressing) has been previously observed/characterized.[27,37] It is the essential role of the HTL/ITO interface in dictating the electron injection and thus necessarily-paired Ag oxidation that has always been overlooked.

After replacing Ag with more electrochemically stable Au **(Fig. 4a, right)**, the back Au electrode is unlikely to oxidize because Au possess higher oxidation potentials than $I_X^-$.[65] $I_X^-$ tends to be oxidized first, producing oxidized iodine species, such as $I_i^0$ and $I_i^+$.[23,37] It is notable that the $I_i^0$ could form $I_2$ that escapes from the perovskite to cause irreversible device performance loss, whereas the $I_i^+$ species could diffuse and/or drift within the perovskite layer to the cathodically-biased ITO side, until they are electrochemically reduced into $I_X^-$ (or $I_i^-$). The observation of iodide oxidation (rather than Au oxidation) has been reported in an analytical study by Xu *et al.* where they observed negligible Au signal via ToF-SIMS, but instead obvious halide segregation via PL spectroscopy in the Au-based perovskite solar cells following reverse bias stressing.[37] We conducted XPS measurements to probe the Au/BCP/$C_{60}$ contact (**Supplementary Fig. 40b**), and we observed negligible binding energy shift associated with Au 4f following reverse bias stressing, consistent with an absence of Au electrochemistry. Furthermore, as distinct from Ag electrode-based cells, our ToF-SIMS depth profiling found no evidence of Au oxidation, as we observed no detectable changes between the unstressed cell and cells stressed at different reverse bias/current (**Supplementary Fig. 39**). Thus, we conclude that the use of more electrochemically stable electrodes should support improved stability under reverse bias. Although Au is likely undesirable for scaled devices, there are a number of alternative electrode materials that should be superior to Ag, such as carbon and TCOs.

## Conclusions

In summary, we systematically investigated factors that could affect the reverse bias behavior of p-i-n structured perovskite solar cells, ranging from passivation of halide vacancies and inserting an additional ETL, to systematically varying the HTLs and metal electrodes. Our results suggest that optimization of the HTLs and selection of electrochemically stable electrodes is of vital importance for preventing reverse bias-driven degradation of perovskite solar cells. Even in the presence of a more reactive Ag electrode, using a robust PTAA HTL improves the average $V_{rb}$ to -7.6 V, as compared with that of -1 V for MeO-2PACz based perovskite solar cells. Further optimization on the metal electrode via replacing Ag with Au extends the average $V_{rb}$ to exceed -15 V. The optimized perovskite solar cells demonstrate recoverable performance loss after stressing at -7 V for 9 hours both in the dark and under partial illumination, as well as good resilience to multiple-cycle stressing tests. Our results suggest that efforts to achieve high reverse bias stability in manufactured perovskite p-i-n devices should focus on (1) using electrodes that are more electrochemically inert (not just limited to Au, but carbon or TCOs); (2) using interlayers that can more robustly block hole and/or electron injection under reverse bias; (3) optimizing the processing of each functioning layers to avoid pinholes or otherwise defective sites that might cause leakage or shunting of the device. Using these strategies, the optimization of the perovskite device architecture could allow realization of large-area p-i-n perovskite solar cells with $V_{rb}$ comparable to silicon PV technologies. This work shows that the reverse bias stability of perovskite optoelectronics, including not just solar cells but also light-emitting diodes and radiation detectors, can be further enhanced by engineering the perovskite and other functional layers to prevent redox reactions.

**Acknowledgments**

This work, and the roles of F.J., Y.S, D.P.M, J.A.S., M.G.C., H.C., S.B., S.R.M, H.J.S., and D.S.G. were primarily supported by the Office of Naval Research (Award # N00014-20-1-2587). F.J. and D.S.G. acknowledge the institutional support from the B. Seymour Rabinovitch Endowment and the state of Washington. The authors acknowledge the use of facilities and instruments at the Photonics Research Center (PRC) at the Department of Chemistry, University of Washington, as well as that at the Research Training Testbed (RTT), part of the Washington Clean Energy Testbeds system. Part of this work was carried out at the Molecular Analysis Facility (MAF), a National Nanotechnology Coordinated Infrastructure site at the University of Washington which is supported in part by the National Science Foundation (NNCI-1542101, NNCI-2025489), the Molecular Engineering & Sciences Institute, and the Clean Energy Institute. We also acknowledge Samantha L. Young from MAF for conducting the XPS measurements. I.G, D.M. and M.D.M acknowledge support by the U.S. Department of Energy's Office of Energy Efficiency and Renewable Energy (EERE) under Solar Energy Technologies Office (SETO) Agreement Number DE-EE0009513. T.R.R. and J.D.M. acknowledge support from the Washington Research Foundation, the University of Washington Clean Energy Institute's Washington Clean Energy Testbeds, and the Department of Energy's SETO through the Perovskite Photovoltaic Accelerator for Commercializing Technologies program. ToF-SIMS analysis was carried out with support provided by the National Science Foundation CBET-1626418. This work conducted in part using resources of the Shared Equipment Authority at Rice University. F.J. especially acknowledges Dr. Jiajie Guo (University of Washington) for Labview programing, Dr. Shinya E. Chen (University of Washington), Dr. Ross Kerner (National Renewable Energy Laboratory), Mr. and Samuel A. Johnson (University of Colorado, Boulder) for all scientific discussions.

**Author contributions**

F.J. and D.S.G. conceived the project, designed the experiments, and discussed the results together. F.J. performed the experiments and analyzed the data. Y.S. performance the AFM, XRD and profilometer measurements, as well as contributed largely to the data processing/analysis. M.Y.Y conducted the SEM measurements. T.R.R. and J.D.M. synthesized and provided $NiO_X$. D.P.M., S.B., and S.R.M. provided the NDI-1 electron transporting material. D.M., I.G., M.D.M., and A.D.M. contributed to the electric field screening calculation and discussions. T.T., F.M. and A.D.M contributed to the ToF-SIMS measurements and discussions. J.A.S., M.G.C. and H.J.S. helped with the standardization of *J-V* characterizations and definition of breakdown voltage. H.C. helped with the data analysis. All authors contributed to the interpretation of the data as well as the presentation of this manuscript. All authors approved the submission. F.J. wrote the first draft. F.J., M.D.M and D.S.G. revised the manuscript with input from all the authors.

## Ethics declarations

Competing interests

M.D.M. is an advisor to Swift Solar. H.J.S. is a co-founder, CSO and a director of Oxford PV. The other authors declare no competing interests.

## Data Availability

All data are available in the main texts or supplementary information. The raw data supporting Figs. 1 - 3 are publicly available in the figshare repository, as part of this record: https://doi.org/10.6084/m9.figshare.24069768. All raw data supporting Figs in the Supplementary Information are available on request.

## Code Availability

All codes and post analysis tools are available on request.

## References


1. Best Research-Cell Efficiency Chart. https://www.nrel.gov/pv/cell-efficiency.html.

2. Lee, M. M. *et al.* Efficient Hybrid Solar Cells Based on Meso-Superstructured Organometal Halide Perovskites. *Science* **338**, 643–647 (2012).

3. Jeon, N. J. *et al.* Solvent Engineering for High-Performance Inorganic–Organic Hybrid Perovskite Solar Cells. *Nat. Mater.* **13**, 897–903 (2014).

4. Yang, W. S. *et al.* Iodide Management in Formamidinium-Lead-Halide–based Perovskite Layers for Efficient Solar Cells. *Science* **356**, 1376–1379 (2017).

5. Lu, H. *et al.* Vapor-Assisted Deposition of Highly Efficient, Stable Black-Phase $FAPbI_3$ Perovskite Solar Cells. *Science* **370**, eabb8985 (2020).

6. Jeon, N. J. *et al.* Compositional Engineering of Perovskite Materials for High-Performance Solar Cells. *Nature* **517**, 476–480 (2015).

7. Yang, W. S. *et al.* High-Performance Photovoltaic Perovskite Layers Fabricated through Intramolecular Exchange. *Science* **348**, 1234–1237 (2015).

8. Li, X. *et al.* A vacuum flash–assisted solution process for high-efficiency large-area perovskite solar cells. *Science* **353**, 58–62 (2016).

9. Zhou, H. *et al.* Interface engineering of highly efficient perovskite solar cells. *Science* **345**, 542–546 (2014).

10. Jeong, J. *et al.* Pseudo-halide anion engineering for α-FAPbI3 perovskite solar cells. *Nature* **592**, 381–385 (2021).

11. Li, N. *et al.* Liquid medium annealing for fabricating durable perovskite solar cells with improved reproducibility. *Science* **373**, 561–567 (2021).

12. Khenkin, M. V. *et al.* Consensus statement for stability assessment and reporting for perovskite photovoltaics based on ISOS procedures. *Nat. Energy* **5**, 35–49 (2020).

13. Li, C. *et al.* Rational design of Lewis base molecules for stable and efficient inverted perovskite solar cells. *Science* **379**, 690–694 (2023).

14. Azmi, R. *et al.* Damp heat–stable perovskite solar cells with tailored-dimensionality 2D/3D heterojunctions. *Science* **376**, 73–77 (2022).

15. PV PACT Center. *PACT* https://pvpact.sandia.gov/.

16. Lan, D. *et al.* Combatting temperature and reverse-bias challenges facing perovskite solar cells. *Joule* **6**, 1782–1797 (2022).

17. Wang, C. *et al.* Perovskite Solar Cells in the Shadow: Understanding the Mechanism of Reverse-Bias Behavior toward Suppressed Reverse-Bias Breakdown and Reverse-Bias Induced Degradation. *Adv. Energy Mater.* **13**, 2203596 (2023).

18. Boyd, C. C. *et al.* Understanding Degradation Mechanisms and Improving Stability of Perovskite Photovoltaics. *Chem. Rev.* **119**, 3418–3451 (2019).

19. Razera, R. A. Z. *et al.* Instability of p–i–n perovskite solar cells under reverse bias. *J. Mater. Chem. A* **8**, 242–250 (2020).

20. Bowring, A. R. *et al.* Reverse Bias Behavior of Halide Perovskite Solar Cells. *Adv. Energy Mater.* **8**, 1702365 (2018).

21. Wolf, E. J. *et al.* Designing Modules to Prevent Reverse Bias Degradation in Perovskite Solar Cells when Partial Shading Occurs. *Sol. RRL* **6**, 2100239 (2022).

22. Bogachuk, D. *et al.* Perovskite Photovoltaic Devices with Carbon-Based Electrodes Withstanding Reverse-Bias Voltages up to –9 V and Surpassing IEC 61215:2016 International Standard. *Sol. RRL* **6**, 2100527 (2022).

23. Ni, Z. *et al.* Evolution of Defects during the Degradation of Metal Halide Perovskite Solar Cells under Reverse Bias and Illumination. *Nat. Energy* **7**, 65–73 (2021).

24. Najafi, L. *et al.* Reverse-Bias and Temperature Behaviors of Perovskite Solar Cells at Extended Voltage Range. *ACS Appl. Energy Mater.* **5**, 1378–1384 (2022).

25. Li, W. *et al.* Sparkling Hot Spots in Perovskite Solar Cells under Reverse Bias. *ChemPhysMater* **1**, 71–76 (2022).

26. Qian, J. *et al.* Destructive Reverse Bias Pinning in Perovskite/Silicon Tandem Solar Modules Caused by Perovskite Hysteresis under Dynamic Shading. *Sustain. Energy Fuels* **4**, 4067–4075 (2020).

27. Xu, Z. *et al.* Reverse-Bias Resilience of Monolithic Perovskite/Silicon Tandem Solar Cells. *Joule* **7**, 1992–2002 (2023).

28. Wang, C. *et al.* Abnormal Dynamic Reverse Bias Behavior and Variable Reverse Breakdown Voltage of ETL-free Perovskite Solar Cells. *Sol. RRL* **7**, 2300456 (2023).

29. Vieira, R. *et al.* A Comprehensive Review on Bypass Diode Application on Photovoltaic Modules. *Energies* **13**, 2472 (2020).

30. Green, M. A. *et al.* Silicon Solar Cells with Integral Bypass Diodes. *Sol. Cells* **3**, 233–244 (1981).

31. Klasen, N. *et al.* A Comprehensive Study of Module Layouts for Silicon Solar Cells Under Partial Shading. *IEEE J. Photovolt.* **12**, 546–556 (2022).

32. Ma, Y. *et al.* Suppressing Ion Migration across Perovskite Grain Boundaries by Polymer Additives. *Adv. Funct. Mater.* **31**, 2006802 (2021).

33. Jeangros, Q. *et al.* In Situ TEM Analysis of Organic–Inorganic Metal-Halide Perovskite Solar Cells under Electrical Bias. *Nano Lett.* **16**, 7013–7018 (2016).

34. Kim, D. *et al.* Light- and Bias-Induced Structural Variations in Metal Halide Perovskites. *Nat. Commun.* **10**, 444 (2019).

35. Bertoluzzi, L. *et al.* Incorporating Electrochemical Halide Oxidation into Drift-Diffusion Models to Explain Performance Losses in Perovskite Solar Cells under Prolonged Reverse Bias. *Adv. Energy Mater.* **11**, 2002614 (2021).

36. Breitenstein, O. *et al.* Understanding Junction Breakdown in Multicrystalline Solar Cells. *J. Appl. Phys.* **109**, 071101 (2011).

37. Xu, Z. *et al.* Halogen Redox Shuttle Explains Voltage-Induced Halide Redistribution in Mixed-Halide Perovskite Devices. *ACS Energy Lett.* **8**, 513–520 (2023).

38. Xu, J. *et al.* Triple-Halide Wide–Band Gap Perovskites with Suppressed Phase Segregation for Efficient Tandems. *Science* **367**, 1097–1104 (2020).

39. Eperon, G. E. *et al.* Metal Halide Perovskite Tandem and Multiple-Junction Photovoltaics. *Nat. Rev. Chem.* **1**, 0095 (2017).

40. Fu, F. *et al.* Monolithic Perovskite-Silicon Tandem Solar Cells: From the Lab to Fab? *Adv. Mater.* **34**, 2106540 (2022).

41. Al-Ashouri, A. *et al.* Monolithic Perovskite/Silicon Tandem Solar Cell with >29% Efficiency by Enhanced Hole Extraction. *Science* **370**, 1300–1309 (2020).

42. Liu, J. *et al.* Efficient and Stable Perovskite-Silicon Tandem Solar Cells through Contact Displacement by $MgF_x$. *Science* **377**, 302–306 (2022).

43. Aydin, E. *et al.* Enhanced Optoelectronic Coupling for Perovskite/Silicon Tandem Solar Cells. *Nature* **623**, 732–738 (2023).

44. Chin, X. Y. *et al.* Interface Passivation for 31.25%-Efficient Perovskite/Silicon Tandem Solar Cells. *Science* **381**, 59–63 (2023).

45. Duan, L. *et al.* Stability Challenges for the Commercialization of Perovskite–Silicon Tandem Solar Cells. *Nat. Rev. Mater.* **8**, 261–281 (2023).

46. Mariotti, S. *et al.* Interface Engineering for High-Performance, Triple-Halide Perovskite–Silicon Tandem Solar Cells. *Science* **381**, 63–69 (2023).

47. Jiang, Q. *et al.* Surface Reaction for Efficient and Stable Inverted Perovskite Solar Cells. *Nature* **611**, 278–283 (2022).

48. Li, L. *et al.* Flexible All-Perovskite Tandem Solar Cells Approaching 25% Efficiency with Molecule-Bridged Hole-Selective Contact. *Nat. Energy* **7**, 708–717 (2022).

49. Shi, Y. *et al.* (3-Aminopropyl)trimethoxysilane Surface Passivation Improves Perovskite Solar Cell Performance by Reducing Surface Recombination Velocity. *ACS Energy Lett.* **7**, 4081–4088 (2022).

50. Taddei, M. *et al.* Ethylenediamine Addition Improves Performance and Suppresses Phase Instabilities in Mixed-Halide Perovskites. *ACS Energy Lett.* **7**, 4265–4273 (2022).

51. Bertoluzzi, L. *et al.* Mobile Ion Concentration Measurement and Open-Access Band Diagram Simulation Platform for Halide Perovskite Solar Cells. *Joule* **4**, 109–127 (2020).

52. Jariwala, S. *et al.* Reducing Surface Recombination Velocity of Methylammonium-Free Mixed-Cation Mixed-Halide Perovskites via Surface Passivation. *Chem. Mater.* **33**, 5035–5044 (2021).

53. Pothoof, J. *et al.* Surface Passivation Suppresses Local Ion Motion in Halide Perovskites. *J. Phys. Chem. Lett.* **14**, 6092–6098 (2023).

54. Akrami, F. *et al.* Kinetic Suppression of Photoinduced Halide Migration in Wide Bandgap Perovskites via Surface Passivation. *J. Phys. Chem. Lett.* **14**, 9310–9315 (2023).

55. Guo, H. *et al.* Immobilizing Surface Halide in Perovskite Solar Cells via Calix[4]pyrrole. *Adv. Mater.* **35**, 2301871 (2023).

56. Boehm, A. M. *et al.* Influence of Surface Ligands on Energetics at $FASnI_3$ /$C_{60}$ Interfaces and Their Impact on Photovoltaic Performance. *ACS Appl. Mater. Interfaces* **12**, 5209–5218 (2020).

57. Al Kurdi, K. *et al.* A Naphthalene Diimide Side-Chain Polymer as an Electron-Extraction Layer for Stable Perovskite Solar Cells. *Mater. Chem. Front.* **5**, 450–457 (2021).

58. Birkhold, S. T. *et al.* Interplay of Mobile Ions and Injected Carriers Creates Recombination Centers in Metal Halide Perovskites under Bias. *ACS Energy Lett.* **3**, 1279–1286 (2018).

59. Phung, N. *et al.* Enhanced Self-Assembled Monolayer Surface Coverage by ALD NiO in p-i-n Perovskite Solar Cells. *ACS Appl. Mater. Interfaces* **14**, 2166–2176 (2022).

60. Paniagua, S. A. *et al.* Phosphonic Acids for Interfacial Engineering of Transparent Conductive Oxides. *Chem. Rev.* **116**, 7117–7158 (2016).

61. Jiang, Y. *et al.* Recent Advances of Synthesis, Properties, Film Fabrication Methods, Modifications of Poly(3,4-ethylenedioxythiophene), and Applications in Solution-Processed Photovoltaics. *Adv. Funct. Mater.* **30**, 2006213 (2020).

62. Li, R. *et al.* Layered Perovskites Enhanced Perovskite Photodiodes. *J. Phys. Chem. Lett.* **12**, 1726–1733 (2021).

63. Tsai, H. *et al.* Addressing the Voltage Induced Instability Problem of Perovskite Semiconductor Detectors. *ACS Energy Lett.* **7**, 3871–3879 (2022).

64. Henzel, J. *et al.* Impact of the Current on Reverse Bias Degradation of Perovskite Solar Cells. *ACS Appl. Energy Mater.* **6**, 11429–11432 (2023).

65. Bard, A. J. *Standard Potentials in Aqueous Solution*. (Routledge, New York, 2017). doi:10.1201/9780203738764.

66. Xu, Z. *et al.* Origins of Photoluminescence Instabilities at Halide Perovskite/Organic Hole Transport Layer Interfaces. *J. Am. Chem. Soc.* **145**, 11846–11858 (2023).

67. Park, S.-J. *et al.* Enhancement of Light Extraction Efficiency of OLEDs Using $Si_3N_4$-based optical scattering layer. *Opt. Express* **22**, 12392 (2014).

68. Sohn, S. *et al.* Printed Organic Light-Emitting Diodes on Fabric with Roll-to-Roll Sputtered ITO Anode and Poly(vinyl alcohol) Planarization Layer. *ACS Appl. Mater. Interfaces* **13**, 28521–28528 (2021).

69. Donie, Y. J. *et al.* Planarized and Compact Light Scattering Layers Based on Disordered Titania Nanopillars for Light Extraction in Organic Light Emitting Diodes. *Adv. Opt. Mater.* **9**, 2001610 (2021).

70. Dykstra, E. *et al.* OLEDs on Planarized Light Outcoupling-Enhancing Structures in Plastic. *Org. Electron.* **111**, 106648 (2022).

71. Guo, F. *et al.* The Fabrication of Color-Tunable Organic Light-Emitting Diode Displays via Solution Processing. *Light Sci. Appl.* **6**, e17094–e17094 (2017).

72. Song, J. *et al.* Organic Light-Emitting Diodes: Pushing Toward the Limits and Beyond. *Adv. Mater.* **32**, 1907539 (2020).

73. Liang, J. *et al.* Origins and Influences of Metallic Lead in Perovskite Solar Cells. *Joule* **6**, 816–833 (2022).

74. Hu, J. *et al.* Organoammonium-Ion-based Perovskites Can Degrade to $Pb^0$ via Amine–Pb(II) Coordination. *ACS Energy Lett.* **6**, 2262–2267 (2021).

75. Lin, W.-C. *et al.* In situ XPS Investigation of the X-ray-triggered Decomposition of Perovskites in Ultrahigh Vacuum Condition. *Npj Mater. Degrad.* **5**, 13 (2021).

76. Bitton, S. *et al.* Perovskite Ionics – Elucidating Degradation Mechanisms in Perovskite Solar Cells *via* Device Modelling and Iodine Chemistry. *Energy Environ. Sci.* **16**, 2621–2628 (2023).

77. Galatopoulos, F. *et al.* Long Thermal Stability of Inverted Perovskite Photovoltaics Incorporating Fullerene-Based Diffusion Blocking Layer. *Adv. Mater. Interfaces* **5**, 1800280 (2018).